The Kimberlites and Related Rocks of the Kuruman Kimberlite Province, Kaapvaal Craton, South Africa

Donnelly, C.L.[1], Griffin, W.L.[1], O'Reilly, S.Y.[1], Pearson, N.J.[1], and Shee, S.R.[2]

1 GEMOC ARC National Key Centre, Department of Earth and Planetary Sciences, Macquarie University, Sydney NSW 2109, Australia.

2 Shee and Associates Pty. Ltd. Glen Iris, VIC 3146, Australia.

Objectives

The Kuruman kimberlite province contains some of the oldest known kimberlites (>1.6 Ga) and was intruded across the margin of the Archean Kaapvaal craton following a major collisional orogeny (ca 1.75 Ga). While most kimberlites intrude a subcratonic lithospheric mantle (SCLM) that has undergone multiple episodes of metasomatism, the Kuruman kimberlites may provide a unique opportunity to examine a relatively undisturbed section of the SCLM across an ancient cratonic margin.

Location

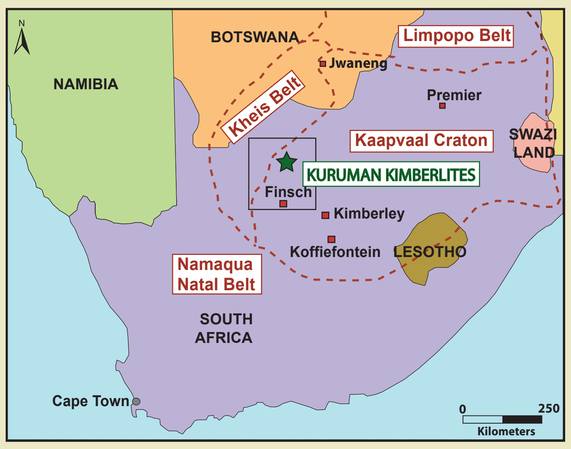

Figure 1. Location of the Kuruman kimberlite province within the Kaapvaal craton.

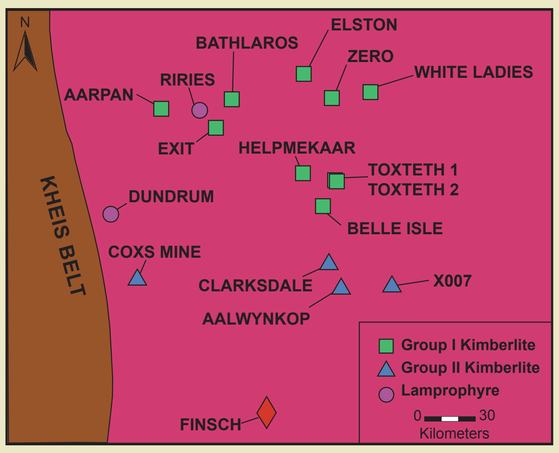

Figure 2. Map showing the location and classification of the kimberlites from the Kuruman Province.

Kimberlite Petrography

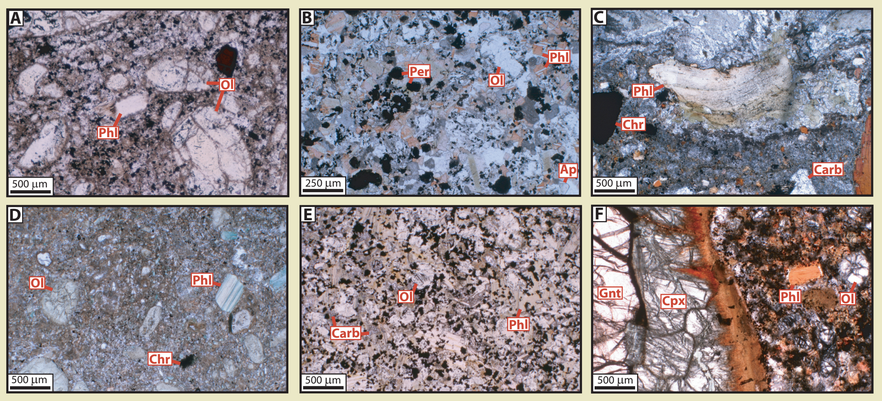

Figure 3. Representative kimberlites from the Kuruman province. (A) Group I kimberlite from Belle Isle, (B) evolved Group I kimberlite from Bathlaros, (C) transitional (lamprophyric) kimberlite from Aalwynkop, (D) Group II kimberlite from X007, (E) opaque-rich Group I kimberlite from White Ladies, and (F) Eclogitic xenolith in a Group I kimberlite from Zero.

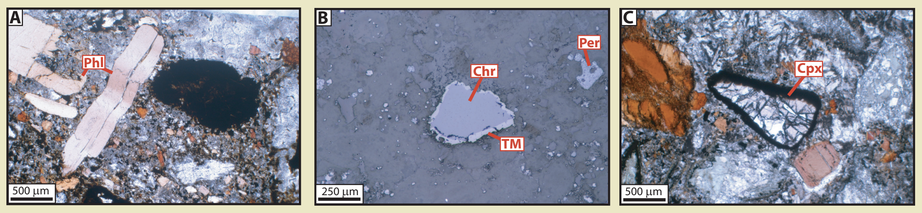

Figure 4. Olivine and phlogopite (Figure 4A) are the most common macrocrystic phases. Macrocrysts of chromite are fairly abundant and are frequently rimmed by titanomagnetite. Clinopyroxene is often present as both macrocryst (Figure 4C) and groundmass phases in transitional kimberlites.

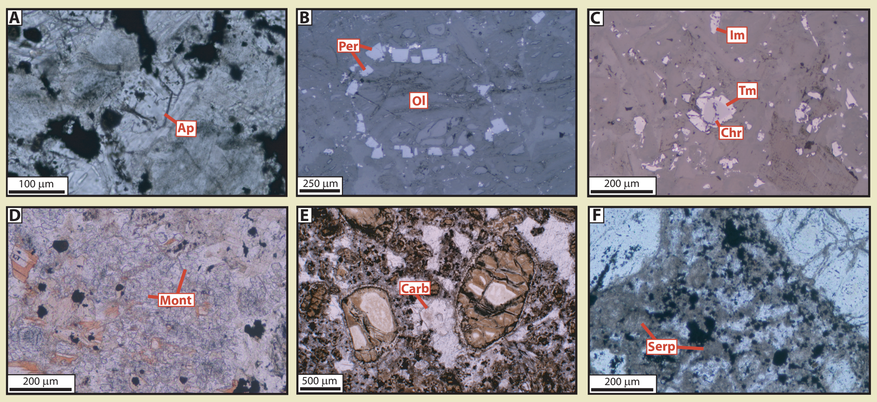

Figure 5. Groundmass minerals include apatite (Figure 5A), perovskite (Figure 5B), ilmenite (Figure 5C), titanomagnetite (Figure 5C) and chromite (Figure 5C). Monticellite (Figure 5D) is commonly present in Group I kimberlites but has been replaced by carbonate. Both primary and secondary carbonate (Figure 5E) and serpentine (Figure 5F) are common groundmass phases.

Kimberlite Mineral Geochemistry

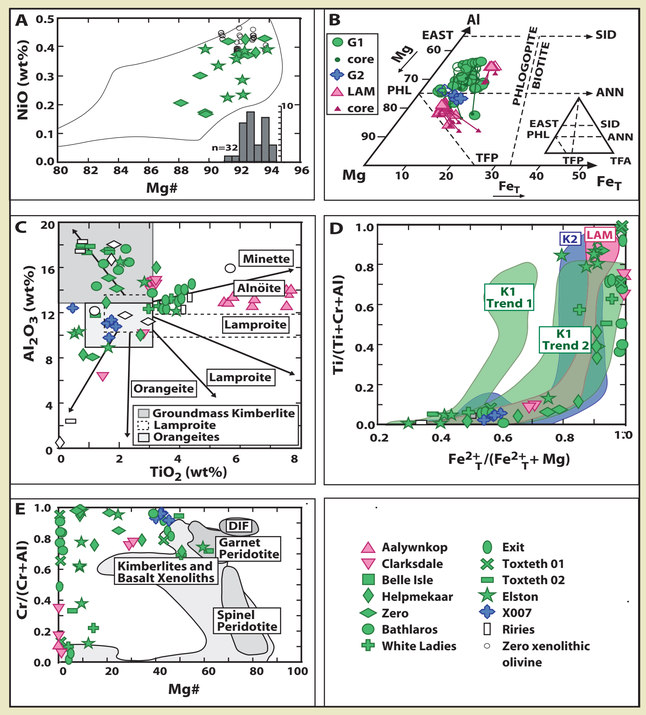

Figure 6. Major-element compositional diagrams for mineral phases from the Kuruman kimberlites: (A) NiO versus Mg# (100Mg/(Mg+Fe)) for olivine; histogram of xenolithic olivine from Shee et al., (1989). Field for kimberlite from Mitchell (1995); (B) mica classifications for the Kuruman kimberlites. Note the different symbols used to represent the different petrographic classifications: open symbols represent phenocrysts and closed symbols represent groundmass grains. Zonation in phologopite grains is shown by lines connecting core compositions (large symbols) to rim compositions (smaller, darker symbols); (C) Al_2O_3 versus TiO_2 for phlogopite; compositional trend lines and fields are from Mitchell (1995). Data for open symobls from Shee et al., (1989); (D) (Ti/(Ti+Cr+Al) versus (Fe^{2+}_T/(Fe^{2+}_T+Mg)) for spinel; Trend 1, Trend 2 fields represent Group I kimberlite trends; K2 represents Group II kimberlite trends and LAM represents lamproite trends from Mitchell (1995); and (E) Cr/(Cr+Al) versus Mg# ((100Mg/(Mg+Fe)) for spinel. Diamond inclusion and peridotite fields are from McDonough and Rudnick (1998) and kimberlite and basalt xenolith fields from Barnes and Roeder (2001).

Kimberlite Geochemistry - Perovskites

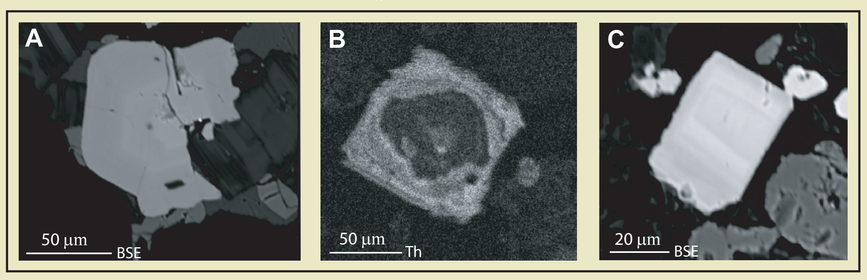

Figure 7. Three styles of perovskite zoning are characterized by (1) a decrease in REE and Th from core to rim (Figure 8A), (2) a less frequently observed reversed pattern (Figure 8B) and (3) a rarely observed, fine-scale, oscillatory pattern (Figure 8C).

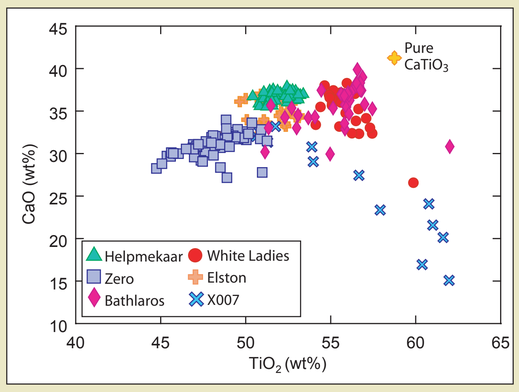

Figure 8. CaO versus TiO_2 (wt%) for perovskites from the Kuruman kimberlite province.

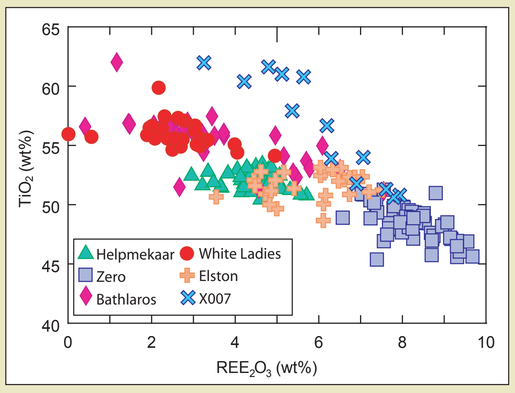

Figure 9. REE_2O_3 (La_2O_3, Ce_2O_3 and Nd_2O_3) content versus TiO_2 (wt%) of groundmass perovskites from the Kuruman kimberlites.

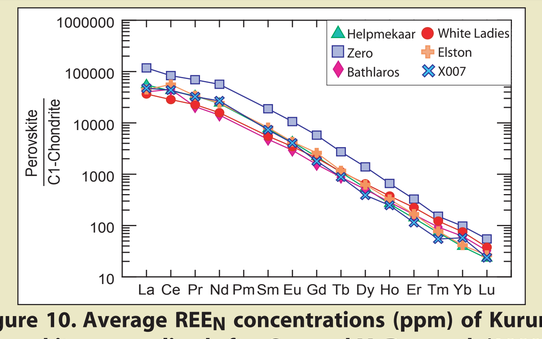

Figure 10. Average REE_N concentrations (ppm) of Kuruman perovskites normalized after Sun and McDonough (1989).

Pipe	Helpmekaar	Zero	Bathlaros	White Ladies	Elston	X007
Na_2O	0.24	1.03	0.48	0.34	0.53	0.65
Cr_2O_3	0.11	0.10	0.37	0.10	0.12	0.60
MnO	≤0.06	0.20	0.10	≤0.06	≤0.06	≤0.06
FeO	2.13	3.02	1.26	1.54	2.06	2.57
Al_2O_3	0.51	0.22	0.13	0.17	0.43	≤0.05
MgO	≤0.08	0.26	0.13	0.19	0.05	1.02
SiO_2	≤0.07	0.25	0.21	0.64	≤0.07	1.59
K_2O	≤0.06	≤0.06	≤0.06	≤0.06	≤0.06	0.18
CaO	36.63	31.00	35.77	35.12	34.94	25.96
TiO_2	52.02	48.23	55.46	55.87	51.57	56.36
NiO	≤0.08	≤0.08	≤0.08	≤0.08	≤0.08	≤0.08
Nb_2O_3	0.92	3.23	0.76	0.57	1.34	1.07
La_2O_3	1.09	1.99	0.87	0.62	1.30	1.39
Ce_2O_3	2.44	4.62	1.88	1.44	3.23	3.36
SrO	0.47	0.46	0.54	0.41	0.48	0.48
Nd_2O_3	0.87	1.65	0.64	0.55	1.24	1.26
Total	97.53	96.32	98.65	97.65	97.40	96.56
Selected Trace Elements (ppm)						
Rb	4	16	25	13	10	115
Y	262	466	353	331	284	171
Nb	8315	32252	9395	4694	13858	8667
Ba	446	1036	833	583	285	1674
Hf	209	226	53	52	113	198
Ta	449	1821	527	581	1109	1078
Pb	368	1699	638	491	1131	124
Th	2213	9264	4536	3167	7341	5870
U	185	452	295	212	201	160

Table 1. Averaged major- (EMPA, wt%) and trace-element (LAM-ICPMS, ppm) contents of Kuruman perovskites.

Sr and Nd Isotopes

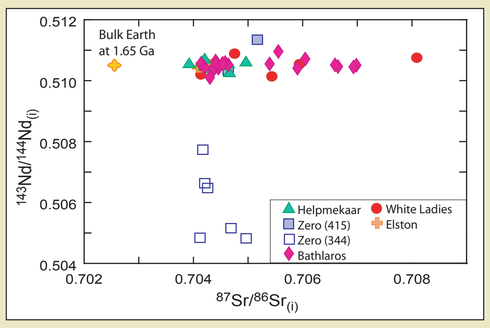

Figure 11. Initial $^{143}Nd/^{144}Nd$ and $^{87}Sr/^{86}Sr$ contents of the Kuruman groundmass perovskites compared with estimated Bulk Earth at 1.65 Ga.

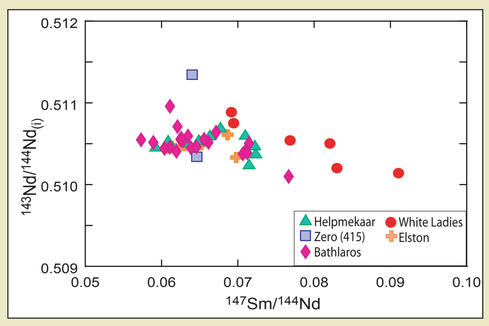

Figure 12. Sm-Nd isotope sytematics of perovskites from the Kuruman kimberlites. Excludes anomalous Zero (344) data.

U-Pb-Th Isotopes

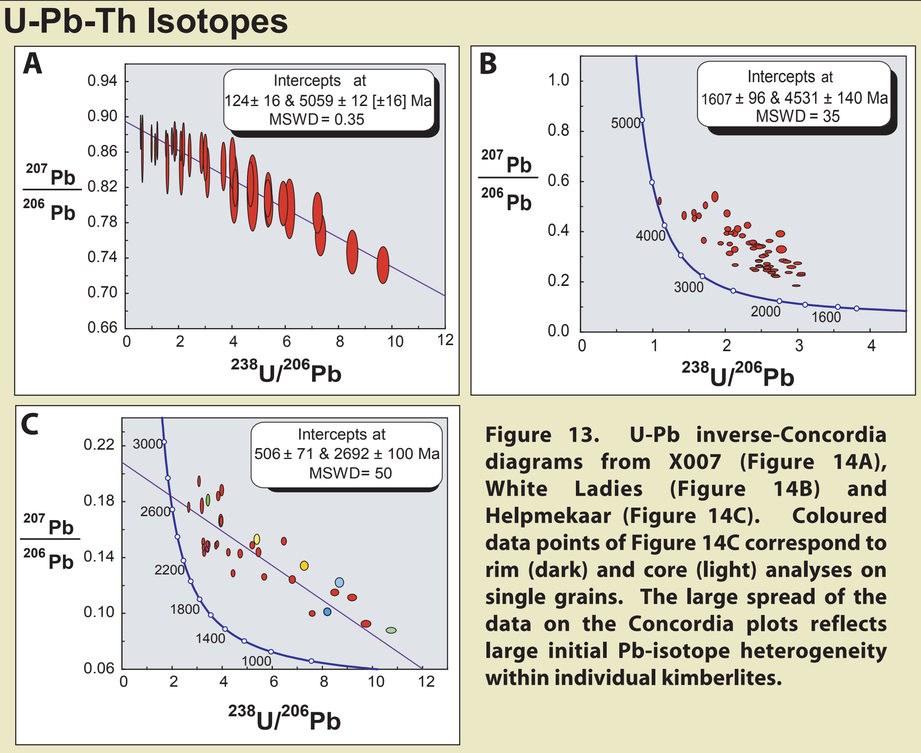

Figure 13. U-Pb inverse-Concordia diagrams from X007 (Figure 14A), White Ladies (Figure 14B) and Helpmekaar (Figure 14C). Coloured data points of Figure 14C correspond to rim (dark) and core (light) analyses on single grains. The large spread of the data on the Concordia plots reflects large initial Pb-isotope heterogeneity within individual kimberlites.

Pipe	Age (Ma)	Upper Intercept (Ma)	MSWD
Helpmekaar	1303 ±190	3052 ± 320	5.9
Zero	1147 ±240	3213 ± 280	17
Bathlaros	506 ±71	2692 ± 100	50
White Ladies	1607 ± 96	4531 ± 140	35
Elston	1265 ±220	3295 ± 320	11
X007	126 ±16	5059 ± 12	0.35

Table 2. U-Pb ages from the Kuruman perovskites. Large age errors and MSWDs are obtained for all pipes, excepting X007, and the upper intercept "ages" (the $^{207}Pb/^{206}Pb$ of the initial Pb component) are unrealistically low. The measured ages are therefore unrealistic, with the exception of White Ladies and X007.

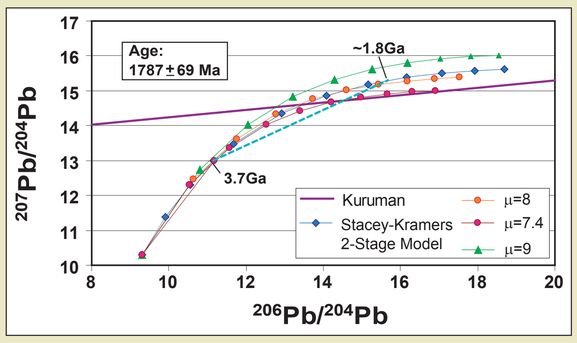

Figure 14. Pb-Pb-isochron plot of all of the Kuruman data (excepting X007) yielding a mean age of 1787 ± 69 Ma; this corresponds to a μ value of 7.4 relative to the two-stage Stacey-Kramers model.

Preliminary Conclusions

- **The Kuruman kimberlites change in petrographic character from east to west and to the south.**
- **Silicate and oxide minerals broadly follow established trends.**
- **Perovskites from the Kuruman kimberlites are unusual having extreme enrichment in REE of up to ~10 wt% and high Th contents.**
- **Preliminary Sr and Nd analyses in perovskite yield values similar to, but slightly more radiogenic than, the Bulk Earth at 1.65 Ga.**
- **Excepting X007, the U-Pb systematics of the perovskites are complicated by high Th contents and large isotopic heterogeneities.**
- **The heterogeneous initial Pb compositions may reflect some form of multi-component mixing before and during perovskite crystallization.**

References

Barnes, S.J., and Roeder, P.L., 2001. The range of spinel compositions in terrestrial mafic and ultramafic rocks. Journal of Petrology 42, 2279-2302.

McDonough, W.F., and Rudnick, R.L., 1998. Mineralogy and composition of the upper mantle. In: Hemley, R. (ed), Ultrahigh-Pressure Mineralogy: Physics and Chemistry of the Earth's Deep Interior. Reviews in Mineralogy 37, 138-164.

Mitchell, R.H.,1995. Kimberlites, Orangeites and Related Rocks. Plemum Press, New York, p. 410.

Shee, S.R., Bristow, J.W., Bell, D.R., Smith, C.B., Allsopp, H.L., and Shee, P.B., 1989. The petrology of kimberlites, related rocks and associated mantle xenoliths from the Kuruman Province, South Africa. 4th IKC volume, Geological Society of Australia, Special Publication 14, 60-82.

Stacey, J.S., and Kramers, J.D. , 1975. Approximation of terrestrial lead isotope evolution by a two-stage model. Earth and Planetary Science Letters 26, 207-221.

Sun, S.-S., and McDonough, W.F., 1989. Chemical and isotopic systematics of oceanic basalts: implications for mantle compositions and processes. In: Sanders, A.D., and Norry, M.J. (eds), Magmatism in the Ocean Basins. Geological Society, London, Special Publications 42, 313-345.